AGU PUBLICATIONS

Geophysical Research Letters

RESEARCH LETTER
10.1002/2016GL068509

Key Points:
- Spatial extent of storms reduces as temperatures increase
- Storm patterns are less uniform at higher temperatures
- Moisture is redistributed from the storm boundaries to the storm center

Supporting Information:
- Supporting Information S1

Correspondence to:
A. Sharma,
a.sharma@unsw.edu.au

Citation:
Wasko, C., A. Sharma, and S. Westra (2016), Reduced spatial extent of extreme storms at higher temperatures, *Geophys. Res. Lett.*, *43*, 4026–4032, doi:10.1002/2016GL068509.

Received 1 MAR 2016
Accepted 5 APR 2016
Accepted article online 7 APR 2016
Published online 25 APR 2016

Reduced spatial extent of extreme storms at higher temperatures

Conrad Wasko[1], Ashish Sharma[1], and Seth Westra[2]

[1]School of Civil and Environmental Engineering, University of New South Wales, Sydney, New South Wales, Australia, [2]School of Civil, Environmental and Mining Engineering, University of Adelaide, Adelaide, South Australia, Australia

Abstract Extreme precipitation intensity is expected to increase in proportion to the water-holding capacity of the atmosphere. However, increases beyond this expectation have been observed, implying that changes in storm dynamics may be occurring alongside changes in moisture availability. Such changes imply shifts in the spatial organization of storms, and we test this by analyzing present-day sensitivities between storm spatial organization and near-surface atmospheric temperature. We show that both the total precipitation depth and the peak precipitation intensity increases with temperature, while the storm's spatial extent decreases. This suggests that storm cells intensify at warmer temperatures, with a greater total amount of moisture in the storm, as well as a redistribution of moisture toward the storm center. The results have significant implications for the severity of flooding, as precipitation may become both more intense and spatially concentrated in a warming climate.

1. Introduction

Short-duration extreme precipitation is predicted to intensify as a result of increases in atmospheric temperature in most locations globally [*Kirtman et al.*, 2013]. Investigation of the historical sensitivity of precipitation to temperature is an important source of evidence to understand how extreme precipitation might change in the future [*Collins et al.*, 2013]. In the absence of changes to circulation patterns and relative humidity, thermodynamic factors suggest that extreme precipitation intensity should scale at about 7%/°C as governed by the Clausius-Clapeyron (C-C) relationship, which describes the capacity of the atmosphere to hold moisture [*Trenberth et al.*, 2003; *Westra et al.*, 2014]. Using present-day climate data, short-duration precipitation has been found to scale at rates ranging from C-C to double C-C for temperatures below 24°C [*Lenderink and van Meijgaard*, 2008; *Hardwick Jones et al.*, 2010; *Lenderink et al.*, 2011; *Mishra et al.*, 2012; *Berg et al.*, 2013], with the scaling differing with storm duration [*Panthou et al.*, 2014; *Wasko et al.*, 2015]. Similar rates of scaling have been observed in long-term historical trends of extreme precipitation, supporting the hypothesis that these relationships may be indicative of future climatic conditions [*Westra and Sisson*, 2011; *Fujibe*, 2013; *Westra et al.*, 2013, 2014].

A mechanism that has been put forward to explain departures from the thermodynamic (C-C) scaling rate is a change in storm dynamics. This has been attributed to the release of latent heat, which can result in the storm increasing the area over which it sources moisture [*Trenberth et al.*, 2003]. Observation of scaling rates above C-C has led to conjecture that there may be changes in dominant precipitation types as convective events have greater scaling rates than nonconvective events [*Haerter and Berg*, 2009; *Berg et al.*, 2013; *Collins et al.*, 2013; *Molnar et al.*, 2015] and also that both the thermodynamic and dynamical mechanisms may operate jointly [*Lenderink and van Meijgaard*, 2008; *Collins et al.*, 2013; *Wasko and Sharma*, 2015] enhancing the convergence of moisture possibly from a larger "moisture source" area [*Trenberth et al.*, 2003; *Westra et al.*, 2014].

The specific causes of changes in precipitation intensity with temperature can therefore be expected to be associated with distinct temporal and spatial signatures. For example, if thermodynamic factors dominate and the precipitation intensifies in proportion to the water-holding capacity of the atmosphere, a consistent increase in precipitation intensity across a storm could be expected. In contrast, if dynamic factors dominate, the spatial extent of each storm cell and the organization of rainfall within the storm cell should change [*Westra et al.*, 2014]. Although evidence exists of intensifying temporal patterns at higher temperatures [*Wasko and Sharma*, 2015], studies investigating possible changes to the spatial signature of storms with climate change remain limited having focused on areal reduction factors for engineering applications [*Li et al.*, 2015] and spatial structures in regional climate models [*Guinard et al.*, 2015].

Here we investigate the relationship between the spatial organization of moisture within a storm and the near-surface dry-bulb temperature. We first examine the hypothesis that the distribution of precipitation with distance from the storm centers differs when storms are stratified by temperature. Subsequently, we examine the relationship with temperature of a range of statistics that describe the organization of moisture within the storm. Finally, using the derived relationships, we develop projections of precipitation distribution with distance from the storm center for higher temperatures.

2. Data and Methods

Subdaily precipitation and 1.2 m dry-bulb temperature were obtained from the Australian Bureau of Meteorology weather station data set and have been used extensively in previous studies [*Hardwick Jones et al.*, 2010; *Westra and Sisson*, 2011; *Westra et al.*, 2012; *Wasko and Sharma*, 2015]. Precipitation is measured using a tipping bucket rain gauge or pluviograph and reported every 6 min. In this study the reported precipitation was accumulated to resolutions of 1 and 3 h. The temperature data resolution is typically 3 to 12 h, depending on the station. The data set contains over 1300 precipitation stations and approximately 1700 temperature stations across Australia.

To analyze the spatial distribution of moisture within a storm, point observations of precipitation need to be transformed to spatial fields. First, at each gauge location, independent precipitation events were identified. Storm events were defined as independent if they were separated by 5 h of zero precipitation for the hourly rainfall series and 15 h of zero precipitation for the 3-hourly rainfall series [*Wasko and Sharma*, 2014]. The precipitation chosen for further analysis was the maximum 1 h or 3 h precipitation burst with each storm. Each precipitation maximum was matched to the coincident temperature, which was calculated as a 24 h moving average centered on the time of the maximum precipitation. The precipitation-temperature pairs were extended to a spatial field by finding the precipitation that occurred at the same time as the maximum from the central gauge at neighboring gauges up to a radius of 50 km. A spatial field was considered for analysis if it had a minimum of five data points and the maximum precipitation in the spatial field occurred at the central gauge. All other spatial fields were discarded. For a station to be included in the analysis it had to have a minimum of 10 years of record length and a minimum of 100 observed independent spatial fields. In total, 93 stations were considered for the 1 h duration and 78 stations for the 3 h duration.

To isolate extreme events, a 90th percentile exponential quantile regression was fitted to the peak precipitation-temperature pairs [*Wasko and Sharma*, 2014] and only spatial field events that exceeded the regression line were analyzed for their sensitivity to temperature. The final data set for each site contains $j = 1..m$ spatial fields matched to their coincident temperature T_j. Each spatial field j contains $i = 1..n$ precipitation observations p_i at distance d_i from the center gauge; thus, p_{ij} is the precipitation observation i of spatial field j.

A set of statistics was chosen to represent the spatial organization of moisture within the spatial fields and calculated on the final m extreme sets of spatial fields. The statistics are as follows:

1. Peak precipitation (PP), which is the maximum precipitation within the spatial field (therefore by definition located at the storm center);
2. Total precipitation (PT), which is the two-dimensional integration of the precipitation plotted against the radial distance from the storm center;
3. Fraction of zero rainfall observations (PZ) in the spatial field;
4. Coefficient of variation (CV), which is the variance of the observations within the spatial field divided by their mean;
5. Effective radius (RE), defined at the centroid of the precipitation where p_{ij} are the n precipitation observations within the spatial field j with distance d_{ij} from the central gauge:

$$\mathrm{RE}_j = \frac{\sum_{i=1}^{n} p_{ij} d_{ij}}{\sum_{i=1}^{n} p_{ij}}; \tag{1}$$

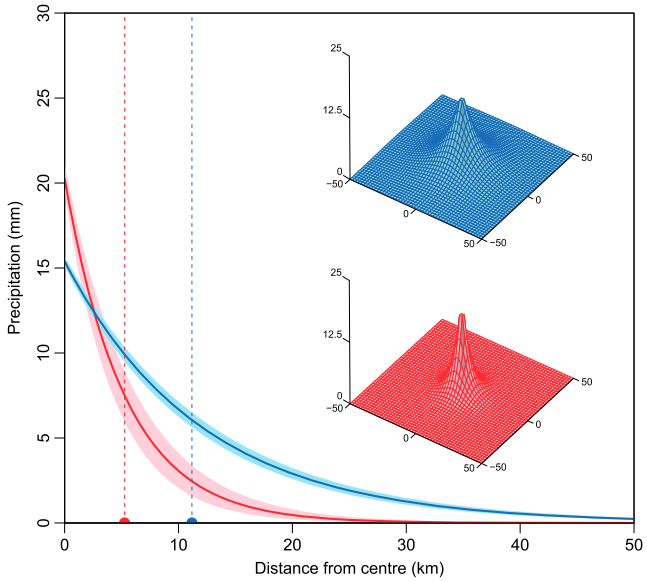

Figure 1. Fitted exponential curves for the greatest 1000 hourly storm bursts by precipitation depth below 18°C (blue) and above 25°C (red). The vertical dashed lines are the corresponding effective radii of the storm data defined as the centroid of the storm by precipitation volume. Three-dimensional curves are also presented emphasizing the increase in the storm intensity at the center of the storm and reduced spatial extent at higher temperatures.

6. Parameters *A* and *B* of an exponential curve that describes how the storm decays with distance from its center [*von Hardenberg et al.*, 2003; *Rebora and Ferraris*, 2006] where the parameters to be estimated for each spatial field *j*:

$$p_{ij}(d_{ij}) = A_j e^{-B_j d_{ij}}. \quad (2)$$

Here *A* and *B* were fitted by minimizing the absolute residuals using a shuffled complex evolution optimization algorithm [*Andrews et al.*, 2011]. A schematic of PP, PT, and RE is presented in Figure S1 in the supporting information.

An exponential regression was then used to find the relationship between each desired statistic set $S_j = \{PP_j, PT_j, CV_j, RE_j, A_j, B_j\}$ with temperature T_j (equation (3)), with the exception of the fraction of zero statistic where a linear regression was used. For a ΔT change in the temperature, the fitted relationship is as follows [*Hardwick Jones et al.*, 2010; *Utsumi et al.*, 2011], where α_s is the rate at which the statistic scales per degree temperature change:

$$S(T + \Delta T) = S(T) \cdot (1 + \alpha_S)^{\Delta T}. \quad (3)$$

The data represent a wide range of climatic zones and precipitation-temperature sensitives [*Hardwick Jones et al.*, 2010; *Utsumi et al.*, 2011; *Wasko and Sharma*, 2014]. The Australian climate can be split into three main zones (Figure 2): tropical in the north, temperate in the east, and arid in the southwest. The precipitation is summer dominant in the tropical north and winter dominant in the subtropical south mainland. Temperate zones in the east have slightly winter-dominant precipitation, with precipitation seasonality becoming uniform toward the south. The scaling of the statistics is aggregated across these climatic zones.

Finally, the spatial fields were projected for a warmer climate on the basis of fitted exponential curves (equation (2)). To represent the current (base) climate, parameters *A* and *B* were calculated at a temperature of 20°C. The curves were then projected in one degree increments using the calculated scaling above (equation (3)). It was found that the scaling of the parameters *A* and *B* was less stable than the peak precipitation (PP) and effective radius (RE) scaling. Hence, the latter were used to scale the fitted curves. The peak precipitation scaling is equivalent to the parameter *A* scaling and the inverse of the effective radius scaling is equivalent to the parameter scaling *B*.

3. Results

3.1. Spatial Organization as a Function of Temperature

In order to confirm the hypothesis that there is a different spatial organization of moisture within storm cells at differing temperature, we begin by splitting all the spatial fields across Australia into two groups: the first for temperatures above 25°C and the second for temperatures below 18°C. If we are able to detect differences in the organization of moisture within the largest storms in these groups, it would suggest that temperature does in fact covary with the spatial signature of storm cells. For both groups the greatest 1000 events by precipitation depth were chosen.

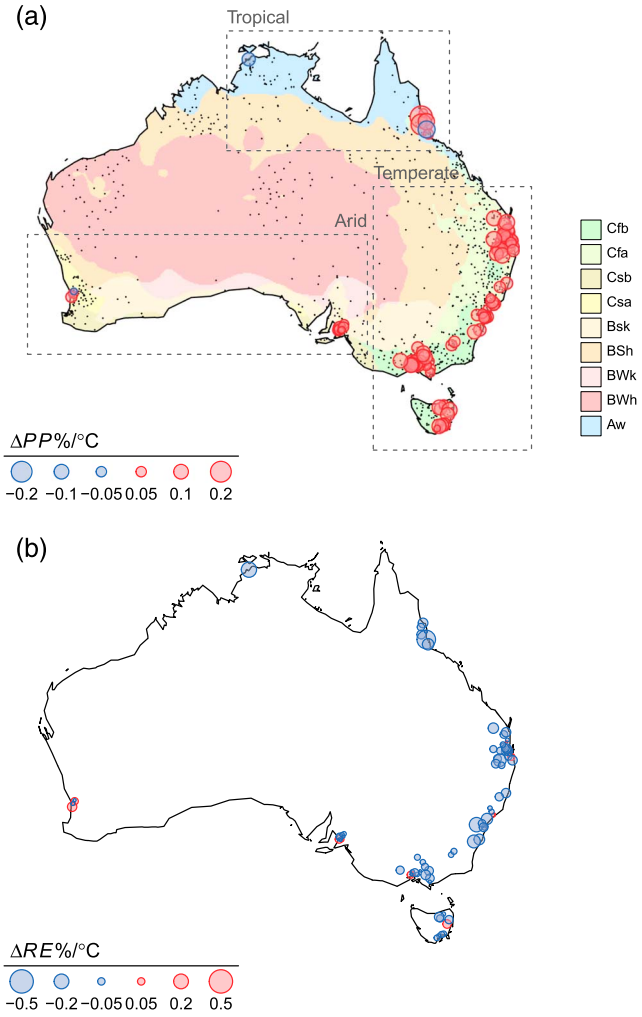

Figure 2. Scaling of the peak precipitation and effective radius for 1 h duration events. Positive scaling is shown in red and negative scaling in blue. (a) Circles show the scaling of peak precipitation, while the background shading denotes the Koppen climate classification [*Peel et al.*, 2007]. General climatic zones are also shown. All the gauge sites used in the analysis are shown as grey dots. (b) Circles show the scaling of effective radius.

Figure 1 presents the calculated exponential curves and the effective radii (equation (2)) of the two groups. The confidence intervals for the parameters A and B were calculated using 1000 bootstrapped replicates of the precipitation data. As can be seen, the intensity at the storm center is greater at high temperatures and decays more rapidly with distance from the center. This indicates that the moisture becomes more concentrated near the storm center for the warmer storms. This is confirmed by considering the effective storm radius: at the higher temperature, the effective storm radius is located closer to the center. Consistent results were found when the analysis was repeated with spatial field aggregated on a regional basis (not shown).

3.2. Scaling of Spatial Field Statistics

Having found that temperature affects the spatial organization of moisture within storm cells, we now focus on the statistics describing the spatial organization for the most extreme events, that is, those above the 90th percentile exponential quantile regression. The scaling of peak precipitation and effective storm radius with temperature for the extreme spatial fields is presented in Figure 2. The peak precipitation increases with temperature at 95% of the sites (Figure 2a), and the effective radius decreases with temperature at 82% of the sites (Figure 2b). An example of the scaling calculations is presented in Figure S2. Consistent increases in the peak precipitation and decreases in the effective radius were found for differing threshold percentiles; however, the magnitude of the scaling was reduced for less extreme threshold percentiles.

The scaling presented in Figure 2 can be grouped by climatic zone and has been presented as box plot distributions in Figure 3. The median scaling of the peak precipitation in the arid zone is approximately 5%°C^{-1}; however, the total storm precipitation scales at a slightly lower rate of approximately 4%°C^{-1}. As the effective radius reduces at higher temperatures this suggests that the precipitation is greater at the storm center and lesser at the storm extents.

This effect is more pronounced for the temperate zone results. The peak precipitation scaling is approximately 7%°C^{-1} and the effective radius has a negative scaling at a median rate of −3%°C^{-1}. Consequently, the scaling in the total precipitation is less than the peak precipitation. This confirms that moisture is being redistributed from the storm boundaries to the storm center, resulting in less precipitation at the storm boundaries and a reduced storm size.

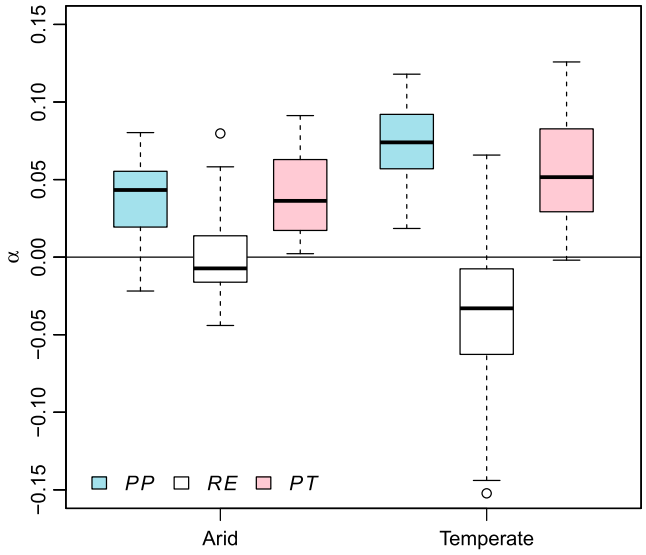

Figure 3. Box plots of peak precipitation scaling, effective radius scaling, and total precipitation scaling for hourly precipitation grouped by arid and temperate zones.

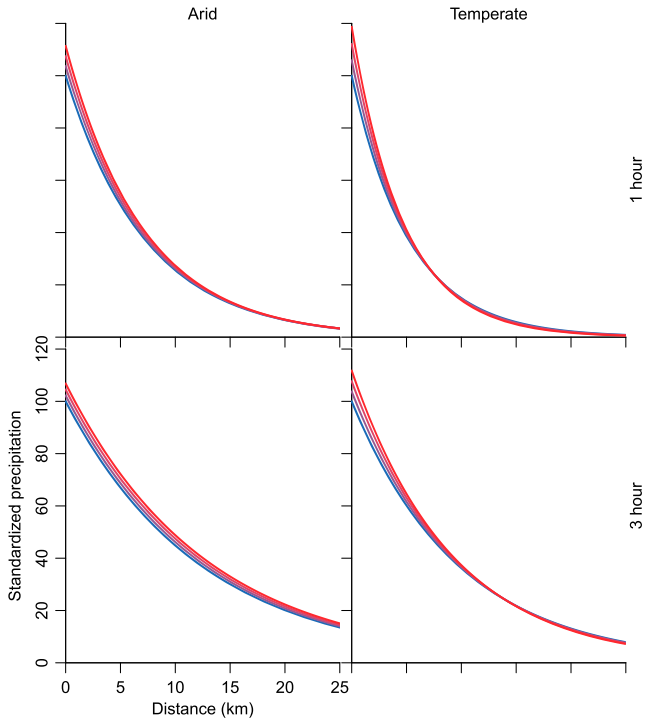

Figure 4. Predicted precipitation distribution due to temperature increase. Each panel consists of four curves. The blue curve is fitted to a temperature of 20°C. Each subsequent curve changes from blue to red in 1°C increments, up to 23°C. The precipitation is standardized by the peak precipitation depth for the baseline climate of 20°C to ensure the results are independent to the baseline temperature choice.

The scaling of the peak precipitation and storm size is stronger at short durations as shown by comparing the 1 h scaling to the 3 h scaling (Figure S3). For 3 h duration bursts, 97% of the sites have positive peak precipitation scaling and 74% of the sites negative effective radius scaling. However, the median scaling of the peak precipitation is reduced to 5%°C^{-1} for the temperate zone and 3%°C^{-1} for the arid zone (Figure S4). Although the median remained similar for the effective radius scaling for the arid zone, in the temperate zone it decreased in magnitude from −3%°C^{-1} for the 1 h duration to −2%°C^{-1} for the 3 h duration storms, suggesting that the redistribution of moisture from the storm boundaries to the storm center is less at longer storm durations.

The scaling of the fraction of observations with zero precipitation (PZ) and the coefficient of variation (CV) in each spatial field also supports the observed trends for the 1 h (Figure S5) and 3 h durations (Figure S6). Throughout Australia, there is a positive scaling in the fraction of zeros and coefficient of variation at 87% and 92% of the sites, respectively, for a 1 h duration. Similar statistics are obtained for a 3 h duration. These results point to a less uniform spatial distribution of precipitation occurring over a smaller area at higher temperatures.

3.3. Projection for Higher Temperatures

Using the scaling relationships developed above, projections were developed to illustrate how the average storm shape for 1 h and 3 durations might change with temperature increases of up to 3°C (Figure 4). The scaling applied is the mean scaling for all the stations within the climatic zone of interest. The blue curve represents the storm shape for a base climate of 20°C and the red curve

represents the shape for a projected increase of 3°C (i.e., 23°C); the intermediate curves represent increases in 1° increments. The precipitation in Figure 4 is standardized by the peak precipitation depth for the baseline climate so the results presented are independent of the baseline temperature choice.

There is minimal change in the storm shape for the arid zone, with an increase in overall precipitation depth occurring at the same rate as the scaling of the peak precipitation regardless of the storm duration. In contrast, in the temperate zone, peak precipitation at the storm center increases at a greater rate than the precipitation at the storm boundaries. In fact there is a decrease in precipitation at the storm boundaries for both 1 h and 3 h duration. This presents the possibility of a smaller storm extent with redistribution of moisture to the storm center at higher temperatures. The redistribution of moisture from the storm boundary to the storm center is less for longer durations (e.g., 3 h), suggesting that the convergence of moisture is more prominent for shorter durations.

4. Conclusions

It is increasingly understood that extreme rainfall scales with atmospheric temperature at or above the Clausius-Clapeyron rate, but how this relates to the spatial organization of events is not well known. The results here show that within a storm burst, precipitation scaling is not spatially uniform, with moisture being redistributed from the storm boundaries to the storm center as temperature increases. Whereas the positive scaling in the total precipitation supports the assertion that the thermodynamic mechanism of increasing moisture capacity dominates increases in precipitation intensity, the redistribution of moisture from the storm boundaries and nonconstant precipitation scaling with radial distance from the storm center suggests that storm dynamics may also be changing. The results therefore suggest that both thermodynamic and dynamic factors result in a storm with greater precipitation intensity with more moisture concentrated at the center. This is consistent with trends from regional climate modeling which predict precipitation structures with larger volume and greater heterogeneity in the future [*Guinard et al.*, 2015]. If the identified historical relationships were to be maintained as global temperatures increase, more concentrated spatial storm events could be expected with higher temperatures. This redistribution could have significant implications for flood severity, as precipitation may become both more intense and spatially concentrated in a warming climate. Future studies will focus on replicating this work using observations from precipitation radars and linking synoptic weather patterns to extreme precipitation patterns to better understand the drivers of precipitation extremes.

Acknowledgments
The authors are grateful for the funding support from the Australian Research Council for this project. Westra was supported by ARC Discovery project DP150100411. The data set can be obtained from http://www.bom.gov.au/climate/data/stations/.

References

Andrews, F. T., B. F. W. Croke, and A. J. Jakeman (2011), An open software environment for hydrological model assessment and development, *Environ. Modell. Software*, *26*(10), 1171–1185, doi:10.1016/j.envsoft.2011.04.006.

Berg, P., C. Moseley, and J. O. Haerter (2013), Strong increase in convective precipitation in response to higher temperatures, *Nat. Geosci.*, *6*(3), 181–185, doi:10.1038/ngeo1731.

Collins, M., et al. (2013), Long-term Climate Change: Projections, Commitments and Irreversibility, in *Climate Change 2013: The Physical Science Basis. Contribution of Working Group I to the Fifth Assessment Report of the Intergovernmental Panel on Climate Change*, edited by T. Stocker et al., pp. 1029–1136, Cambridge Univ. Press, Cambridge U. K., and New York.

Fujibe, F. (2013), Clausius-Clapeyron-like relationship in multidecadal changes of extreme short-term precipitation and temperature in Japan, *Atmos. Sci. Lett.*, *14*(3), 127–132, doi:10.1002/asl2.428.

Guinard, K., A. Mailhot, and D. Caya (2015), Projected changes in characteristics of precipitation spatial structures over North America, *Int. J. Climatol.*, *35*(4), 596–612, doi:10.1002/joc.4006.

Haerter, J. O., and P. Berg (2009), Unexpected rise in extreme precipitation caused by a shift in rain type?, *Nat. Geosci.*, *2*(6), 372–373, doi:10.1038/ngeo523.

Hardwick Jones, R., S. Westra, and A. Sharma (2010), Observed relationships between extreme sub-daily precipitation, surface temperature, and relative humidity, *Geophys. Res. Lett.*, *37*, L22805, doi:10.1029/2010GL045081.

Kirtman, B., et al. (2013), Near-term climate change: Projections and predictability, in *Climate Change 2013: The Physical Science Basis. Contribution of Working Group I to the Fifth Assessment Report of the Intergovernmental Panel on Climate Change*, edited by T. Stocker et al., pp. 953–1028, Cambridge Univ. Press, Cambridge, U. K., and New York.

Lenderink, G., and E. van Meijgaard (2008), Increase in hourly precipitation extremes beyond expectations from temperature changes, *Nat. Geosci.*, *1*(8), 511–514, doi:10.1038/ngeo262.

Lenderink, G., H. Y. Mok, T. C. Lee, and G. J. van Oldenborgh (2011), Scaling and trends of hourly precipitation extremes in two different climate zones—Hong Kong and the Netherlands, *Hydrol. Earth Syst. Sci.*, *15*(9), 3033–3041, doi:10.5194/hess-15-3033-2011.

Li, J., A. Sharma, F. Johnson, and J. Evans (2015), Evaluating the effect of climate change on areal reduction factors using regional climate model projections, *J. Hydrol.*, *528*, 419–434, doi:10.1016/j.jhydrol.2015.06.067.

Mishra, V., J. M. Wallace, and D. P. Lettenmaier (2012), Relationship between hourly extreme precipitation and local air temperature in the United States, *Geophys. Res. Lett.*, *39*, L16403, doi:10.1029/2012GL052790.

Molnar, P., S. Fatichi, L. Gaál, J. Szolgay, and P. Burlando (2015), Storm type effects on super Clausius–Clapeyron scaling of intense rainstorm properties with air temperature, *Hydrol. Earth Syst. Sci.*, *19*(4), 1753–1766, doi:10.5194/hess-19-1753-2015.

Panthou, G., A. Mailhot, E. Laurence, and G. Talbot (2014), Relationship between surface temperature and extreme rainfalls: A multi-time-scale and event-based analysis, *J. Hydrometeorol.*, *15*(5), 1999–2011, doi:10.1175/JHM-D-14-0020.1.

Peel, M., B. Finlayson, and T. McMahon (2007), Updated world map of the Köppen-Geiger climate classification, *Hydrol. Earth Syst. Sci.*, *11*, 1633–1644.

Rebora, N., and L. Ferraris (2006), The structure of convective rain cells at mid-latitudes, *Adv. Geosci.*, *7*, 31–35.

Trenberth, K. E., A. Dai, R. M. Rasmussen, and D. B. Parsons (2003), The changing character of precipitation, *Bull. Am. Meteorol. Soc.*, *84*(9), 1205–1217, doi:10.1175/BAMS-84-9-1205.

Utsumi, N., S. Seto, S. Kanae, E. E. Maeda, and T. Oki (2011), Does higher surface temperature intensify extreme precipitation?, *Geophys. Res. Lett.*, *38*, L16708, doi:10.1029/2011GL048426.

von Hardenberg, J., L. Ferraris, and A. Provenzale (2003), The shape of convective rain cells, *Geophys. Res. Lett.*, *30*(24), 2280, doi:10.1029/2003GL018539.

Wasko, C., and A. Sharma (2014), Quantile regression for investigating scaling of extreme precipitation with temperature, *Water Resour. Res.*, *50*, 3608–3614, doi:10.1002/2013WR015194.

Wasko, C., and A. Sharma (2015), Steeper temporal distribution of rain intensity at higher temperatures within Australian storms, *Nat. Geosci.*, *8*(7), 527–529, doi:10.1038/ngeo2456.

Wasko, C., A. Sharma, and F. Johnson (2015), Does storm duration modulate the extreme precipitation-temperature scaling relationship?, *Geophys. Res. Lett.*, *42*, 8783–8790, doi:10.1002/2015GL066274.

Westra, S., and S. A. Sisson (2011), Detection of non-stationarity in precipitation extremes using a max-stable process model, *J. Hydrol.*, *406*(1–2), 119–128, doi:10.1016/j.jhydrol.2011.06.014.

Westra, S., R. Mehrotra, A. Sharma, and R. Srikanthan (2012), Continuous rainfall simulation: 1. A regionalized subdaily disaggregation approach, *Water Resour. Res.*, *48*, W01535, doi:10.1029/2011WR010489.

Westra, S., L. Alexander, and F. Zwiers (2013), Global increasing trends in annual maximum daily precipitation, *J. Clim.*, *26*, 3904–3918, doi:10.1175/JCLI-D-12-00502.1.

Westra, S., H. J. Fowler, J. P. Evans, L. Alexander, P. Berg, F. Johnson, E. J. Kendon, G. Lenderink, and N. M. Roberts (2014), Future changes to the intensity and frequency of short-duration extreme rainfall, *Rev. Geophys.*, *52*, 522–555, doi:10.1002/2014RG000464.